Intermolecular Raman spectroscopy of long-range interactions: The CO_2-Ar collision-induced ν_3 CO_2 band

M. Chrysos,* F. Rachet, and N. I. Egorova†
Laboratoire des Propriétés Optiques des Matériaux et Applications, UMR CNRS 6136, Université d'Angers, 2 boulevard Lavoisier, 49045 Angers, France

A. P. Kouzov‡
Institute of Physics, Saint Petersburg State University, Ulyanovskaya str. 1, Peterhof, Saint Petersburg 195904, Russia
(Received 27 July 2006; published 9 January 2007)

We report an exhaustive joint theoretical/experimental collision-induced Raman scattering (CIRS) study of the Raman-forbidden ν_3 band of CO_2. Original zeroth and second anisotropic spectral moment formulas for CO_2-Ar are derived, in which complete expressions of Raman amplitudes (derived by the authors with a recently reported universal method [Phys. Rev. A **74**, 012723 (2006)]) are input. The method, applicable to any kind of spectroscopy and whatever the number of photons, molecules, or interaction involved, uses the irreducible spherical tensor formalism in conjunction with a Feynman-like diagrammatic technique to describe any long-range induced property mechanism. Experimentally, spectral moments are deduced from careful, absolute-scale, frequency-resolved CO_2-Ar depolarized CIRS measurements of unprecedented accuracy. From comparison between theory and experiment, we provide quantitative evidence of a substantial contribution of a nonlinear dipole polarization mechanism, predicted theoretically in the preceding paper. In this mechanism, both photons are shown to interact with Ar (which then couples to CO_2 via intermolecular interactions), rather than with both colliders that is the case in the standard dipole-induced quadrupole (DIQ) interaction. The effect had thus far escaped notice possibly because of the reduced accuracy of the earlier self-consistent field dipole-quadrupole polarizablity computations along with a lack of CIRS measurements. In light of recent extensive computations by Haskopoulos and Maroulis [Chem. Phys. Lett. **417**, 235 (2006)], the improved *ab initio* data of these properties are found to corroborate our predictions, and confirm that the Raman amplitude owing to the dipole-dipole-quadrupole hyperpolarizability of the atomic perturber strongly and destructively interferes with the (otherwise dominant) DIQ Raman amplitude.

DOI: 10.1103/PhysRevA.75.012707 PACS number(s): 34.90.+q, 33.20.Ea, 42.65.An, 33.20.Fb

I. INTRODUCTION

Over the last 25 years interaction-induced light scattering has witnessed an impressive progress ([1–3], and references therein). Nowadays, a revival of the topic is being ascertained since this spectroscopy now appears as an effective means to access nonlinear polarizabilities of molecular clusters [4–6]. The need for a fuller understanding of the mechanisms of the pairwise interactions involving nonreactive molecules of atmospheric interest, as well as the ever growing needs of material science (conception and characterization of functional media for specific purposes) may explain why polarizabilities are now taking such a singular place.

Collision-induced Raman scattering (CIRS) is a spectral signature of incremental polarizabilities $\Delta\hat{\alpha}$. The latter are excess quantities defined by

$$\Delta\hat{\alpha} = \hat{\alpha} - (\hat{\alpha}_a + \hat{\alpha}_b + \hat{\alpha}_c + \cdots), \tag{1}$$

where $\hat{\alpha}$ is the total polarizability of the system and $\hat{\alpha}_a, \hat{\alpha}_b, \hat{\alpha}_c, \ldots$, the ones of the independent colliding partners. For molecular pairs *a*-*b*, incremental polarizabilities appear because of the interaction between *a* and *b*. As the latter depend strongly on the intermolecular separation **R**, generated spectra have broad Raman band shapes whose intensity scales as the product $(1-\frac{1}{2}\delta_{a,b})\rho_a\rho_b$ of the molecular densities ρ_a and ρ_b. The degree in which $\Delta\hat{\alpha}(q_a, q_b; \mathbf{R})$ depend on vibrotational coordinates, q_a and q_b, is generally much different from the one exhibited in individual polarizabilities $\hat{\alpha}_a$ and $\hat{\alpha}_b$. Therefore, CIRS bands may appear at transition frequencies that are Raman-inactive in isolated molecules. For instance, the $g \rightarrow u$ transition which is forbidden in centrosymmetric molecules like CO_2 turns out to be allowed in CIRS, and the Raman-inactive ν_2 and ν_3 modes of CO_2 do generate CIRS spectra.

CIRS and its hyper-Raman counterpart allow, in principle, to probe the incremental linear and nonlinear polarizability tensors of a molecular cluster, respectively. However, although the former process is an essentially linear optical response, it turns out that in some cases it may have a nonlinear signature [5,7]. Thus, in pure CO_2, Amos *et al.* [5] interpreted this nonlinear contribution as being due to the permanent quadrupole moment of the molecule, and found the nonlinear term to be insignificant. Recently, it was shown ([8], hereafter referred to as paper I) that nonlinear quadrupole (NLQ) polarization is not the only existing nonlinear mechanism. Another such mechanism appears when *a* has a transition dipole moment μ_a, and *b* has a dipole-dipole-quadrupole hyperpolarizability $\hat{B}_b$. This important result and

*Electronic address: michel.chrysos@univ.angers.fr
†Also at the Institute of Physics, Saint Petersburg State University, Ulyanovskaya str. 1, Peterhof, Saint Petersburg 195904, Russia.
‡Electronic address: alex@AK1197.spb.edu

the formal structure of the new mechanism (hereafter referred to as NLD) were obtained by means of a diagrammatic method capable of depicting, organizing, and classifying the various long-range polarization contributions in a field-matter many-body problem, involving an arbitrary number of photons, molecules, or interactions [8]. Note in passing that, with reference to the diagrammatic theory employed here and in [8], certain light-shift terms, omitted in the early diagrammatic formulations of perturbation theory [9], are also missing from the present development. However, although such terms would seem to contribute formally in second and higher photon orders (for a thorough analysis of these terms, see [10]), they can be safely neglected in the present study, and the same is true for other small effects such as the Doppler shift [11].

According to our theory, scattering cross sections are expected to contain terms that are proportional to the matrix-element product of μ_a and $\hat{B}_b$. Although, quantitatively, the relative contribution of NLD cannot be assessed from the outset, one expects this to be pronounced for molecules with strong infrared-active (IR-active) transitions. The ν_3 transition of CO_2 turns out to be particularly appealing, as developed below. Here, full quantitative evidence of the predicted nonlinear effect is obtained. Furthermore, we show how CIRS spectra can provide data on nonlinear polarization constants and the concomitant vibrational matrix elements, and how these spectra should be used to further improve incremental polarizabilities.

II. THE WORKING SYSTEM

As an active system, the carbon dioxide molecule turned out to assemble several advantages. Its choice was dictated by its importance as an atmospheric compound, and especially as a greenhouse gas. Its linear structure and covalent character at equilibrium turned out to be appreciable properties when polarizabilities are to be studied, whereas its huge and constantly updated scientific literature allowed the use of state-of-the-art properties.

Among the normal modes of CO_2 we opted for stretching. In such a mode, a linear molecule can still be treated as a linear rotator, whereas in the bending mode CO_2 should rather be viewed as a symmetric top. Needless to mention, for a stretching mode there is a considerable gain in simplicity when working out the mathematical structure of an induced property.

The CO_2 molecule has two stretching modes. The ν_1, being symmetric, is Raman-active, while the ν_3, which is antisymmetric, is Raman-inactive. They both are CIRS active, for the reasons developed in Sec. I. In order to isolate the predicted CIRS effect, it was preferable that the standard Raman mechanism is blocked. This is the case of ν_3, a transition activated solely by intermolecular interactions.

On theoretical grounds, the choice of atomic argon as a perturbing gas turned out be far preferable to autoperturbed CO_2. The advantages of CO_2-Ar are twofold. First, a multiproperty optimized, highly accurate CO_2-Ar potential energy surface (PES) [12] has been developed. Second, due to the isotropy of the perturber the Racah algebra in the derivation of $(\Delta\hat{\alpha})_{FI}$ is far less complex than it is for CO_2-CO_2.

On experimental grounds, however, CO_2-Ar turns out to be more difficult to treat. In fact, binary CIRS spectra by mixtures like CO_2:Ar are a superposition of two broad spectra (the one owing to the like CO_2-CO_2 pair and the other owing to the unlike CO_2-Ar pair) that both peak at the studied CO_2 transition frequency and have (qualitatively) similar patterns. Given that CIRS measurements are generally subject to nonnegligible experimental uncertainties, the procedure of subtracting signals in order to extract the useful CO_2-Ar cross section is often unreliable. Despite this inherent technical difficulty, we did manage to extract reliable CO_2-Ar band shapes (see below). This was possible thanks to an experimental setup of exceptional sensitivity (for a detailed description, see Ref. [13]) and to a specific knowhow in detecting and treating particularly weak scattering signals. The quality of the extracted CO_2-Ar absolute-calibrated binary cross sections was checked by studying their degree of stability for various CO_2:Ar concentrations. For this purpose a complete study of the measured signals against ρ_a was needed, with the Raman frequency ν treated as a parameter.

In the following section, a rigorous analysis of the two low-order classical moments of the anisotropic incremental polarizability $(\Delta\alpha^{(2)})_{FI}$ is made, where formal expressions reported in paper I are employed. The tedious mathematical steps have been skipped as a compromise between clarity and sharpness, and the lengthy Racah algebra that was necessary throughout has been developed as succinctly as possible. Some helpful additional technical material can be found in Ref. [14] where different (but somehow analogous) torque spectra relevant to IR/NMR spectroscopy have been treated. The full derivation of the most general moment problem for a pair *a*-*b*, adaptable to any spectroscopy, will be the object of a forthcoming publication. In the remainder, notations that are identical to those in paper I are used; working symbols will not be defined again, unless new symbols or definitions appear or unless otherwise is stated. Raman frequencies (in cm^{-1} units) are denoted by ν, with $\nu=\nu_1-\nu_2$, and ν_1 (ν_2) the frequency of the absorbed (emitted) photon; note that $\nu_1=1/\lambda_L$, where λ_L is the laser wavelength, and that ν_2 corresponds to the frequency probed by the experiment; finally, $\nu-\nu_0$ defines the detuning relative to the ν_3-transition frequency $\nu_0=1/\lambda_0=2350\ cm^{-1}$ [15].

III. THEORETICAL

A. Depolarized CIRS amplitudes and diagrams

1. The dipole-induced quadrupole interaction (DIQ)

DIQ polarization has long been known as the standard dominant long-range mechanism of CO_2-Ar. The relevant multipolar ranks are $l_a=2$, $l_b=1$, and the intermolecular coupling reads $W_{l_a l_b}=W_{21}$. There are $2\times 3!$ diagrams contributing to the scattering amplitude, each involving initial and final states $|i_c\rangle$ and $|f_c\rangle$, and transient virtual states $|k_c\rangle$ $(c=a,b)$. Half of those are shown in Fig. 1. The rest are obtained by interchanging the photon arrows in each of the displayed diagrams. As a particular case of the analysis of paper I, the resulting anisotropic polarizability reads

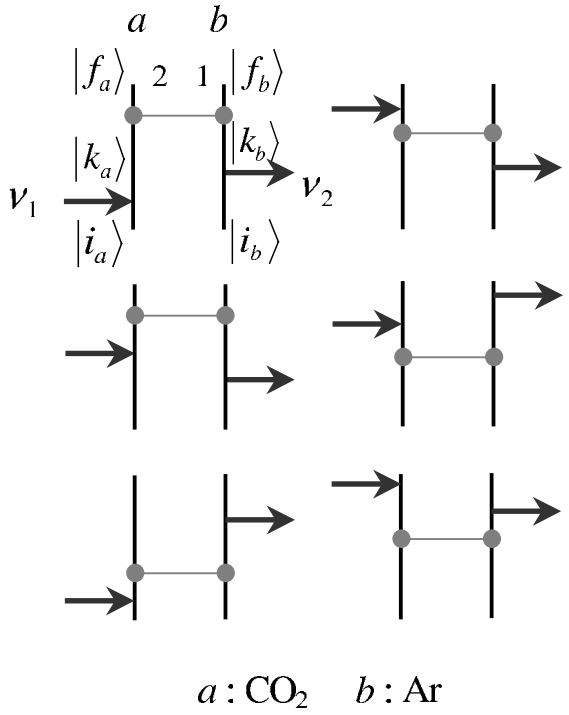

FIG. 1. Half of the Feynman diagrams contributing to the anisotropic DIQ polarizability of CO_2-Ar. Symbols are defined in the text.

$$(\Delta\alpha^{(2)})_{FI} = -\frac{6\sqrt{14}}{5}\alpha_b[(a_{1a})_{f_a i_a}\{C_a^{(1)} \otimes C^{(3)}\}^{(2)} - (a_{3a})_{f_a i_a}\{C_a^{(3)} \otimes C^{(3)}\}^{(2)}]R^{-4} \quad (2)$$

where α_b is the static dipole-dipole polarizability of Ar ($\alpha_b = 11.1a_0^3$), and $a_{1a} = A_{Z,ZZ} + 2A_{X,ZX}$, $a_{3a} = A_{Z,ZZ} - 4A_{X,ZX}/3$ are the invariants of the dipole-quadrupole polarizability of CO_2.

Table I gathers values of matrix elements $(A_{Z,ZZ})_{f_a i_a}$, $(A_{X,ZX})_{f_a i_a}$, $(a_{1a})_{f_a i_a}$, $(a_{3a})_{f_a i_a}$. The entries (in au) were obtained by processing reported self-consistent field (SCF) [5,16] and second-order Moller-Plesset (MP2) [16] *ab initio* computation data.

TABLE I. Values (in au) of the matrix-elements $(A_{Z,ZZ})_{f_a i_a}$, $(A_{X,ZX})_{f_a i_a}$, $(a_{1a})_{f_a i_a}$, $(a_{3a})_{f_a i_a}$. The entries (in au) were obtained by processing reported SCF [5,16] and MP2 [16] *ab initio* computation data.

	Amos *et al.* [5] SCF	Haskopoulos-Maroulis [16] SCF	Haskopoulos-Maroulis [16] MP2
$(A_{Z,ZZ})_{f_a i_a}$	−1.82	−2.11	−2.53
$(A_{X,ZX})_{f_a i_a}$	−0.70	−1.66	−1.90
$(a_{1a})_{f_a i_a}$	−3.22	−5.43	−6.33
$(a_{3a})_{f_a i_a}$	−0.89	0.11	0.00

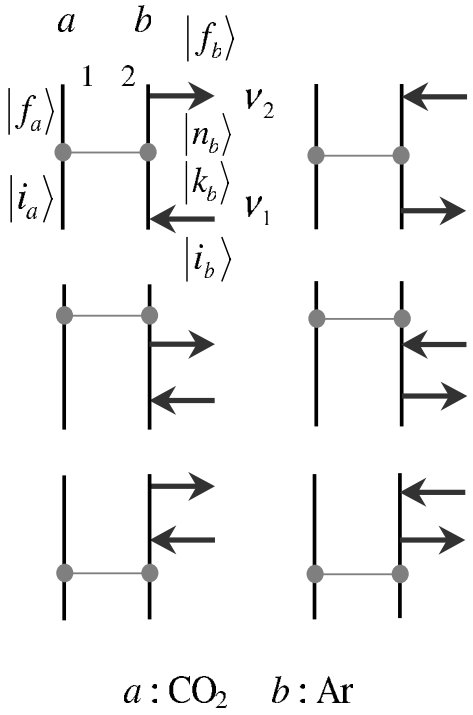

FIG. 2. The six Feynman diagrams that are relevant to the NLD polarization mechanism of CO_2-Ar.

2. The nonlinear dipole-field induction (NLD)

This mechanism, absent in isotropic CIRS but present in depolarized CIRS, had been overlooked in the previous classical treatment [5]. The relevant intermolecular interaction is the dipole-quadrupole coupling $W_{l_a l_b} = W_{12}$ because, here, the vibrating dipole of CO_2 is a source of the internal field. Both photon-lines are attached to the buffer. The scattering amplitude is made of only 3! diagrams, each involving initial and final states $|i_c\rangle$ and $|f_c\rangle$ ($c = a, b$), and a double set of transient virtual states $|k_b\rangle$ and $|n_b\rangle$. These are shown in Fig. 2. For CO_2-Ar, the resulting contribution reads

$$(\Delta\alpha^{(2)})_{FI} = \frac{3}{2}\sqrt{14}B_b(\mu_a)_{f_a i_a}\{C_a^{(1)} \otimes C^{(3)}\}^{(2)}R^{-4} \quad (3)$$

where B_b stands for the $B = B_{ZZ,ZZ}$ isotropic component of the dipole-dipole-quadrupole static hyperpolarizability tensor $\hat{B}$ of Ar ($B = -156$ au [17]), and $(\mu_a)_{f_a i_a} = 0.1264$ au [18] is the transition matrix element of the CO_2 dipole moment μ_z.

Both NLD and DIQ have the same (dominant) R^{-4} asymptotic dependence, which is in itself a remarkable finding. Although formally NLQ (the contribution of which was found to be insignificant in CO_2-CO_2 [5]) also does so, in CO_2-Ar this mechanism is strictly absent because atoms have no dipole-dipole-dipole hyperpolarizability $\hat{\beta}_b$ or permanent quadrupole moment. However, even more striking is the fact that in CO_2-Ar the new NLD mechanism dramatically affects depolarized CIRS spectra. This is what came out from a direct comparison between theoretical and experimental zeroth and second moments.

B. Moments

Classical binary moments $M_{2p}^{(2)}$ $(p=0,1,\ldots)$ are here considered. According to standard definition

$$M_{2p}^{(2)} = \left\langle\!\!\left\langle \left(\frac{d^p}{dt^p}(\Delta\alpha^{(2)})_{FI}, \frac{d^p}{dt^p}(\Delta\alpha^{(2)})_{FI} \right) \right\rangle\!\!\right\rangle \tag{4}$$

where double angular brackets $\langle\langle\ \rangle\rangle$ denote equilibrium average with a binary correlation function kernel

$$G(\mathbf{R},\Omega_a) = \frac{1}{4\pi} \exp\left(-\frac{V}{k_B T} \right). \tag{5}$$

The latter function brings into play $V(\mathbf{R},\Omega_a)$, the anisotropic CO_2-Ar interaction potential [19]. Note that the $1/4\pi$ factor in Eq. (5) ensures proper normalization of integrated quantities over the internal, extra configuration subspace Ω_a. Single brackets are used throughout to denote integration over the configuration space, so that $\langle\langle X\rangle\rangle = \langle XG\rangle = \int\int\int XGR^2 dR d\Omega d\Omega_a$.

The next steps of the analysis consist, first, in expanding $G(\mathbf{R},\Omega_a)$ in Legendre polynomials $P_L(\cos\theta_a')$ (where θ' is the angle between $\mathbf{R}$ and the CO_2-axis unit-vector $\mathbf{n}_a$), and then, in specifying $(\Delta\alpha^{(2)})_{FI}$ for the system worked upon. Formally, $G(\mathbf{R},\Omega_a)$ is given the form

$$\begin{aligned} G(\mathbf{R},\Omega_a) &= \sum_L G_L(R) P_L(\cos\theta_a') \\ &= \sum_L G_L(R) (C^{(L)}(\Omega_a), C^{(L)}(\Omega)), \end{aligned} \tag{6}$$

where the Racah spherical harmonics $C^{(L)}$ have been introduced [20]. For CO_2-Ar, $(\Delta\alpha^{(2)})_{FI}$ reads

$$\begin{aligned} (\Delta\alpha^{(2)})_{FI} = {} & \mathcal{B}_2(1,3;R)\{C_a^{(1)} \otimes C^{(3)}\}^{(2)} \\ & + \mathcal{B}_2(3,3;R)\{C_a^{(3)} \otimes C^{(3)}\}^{(2)}, \end{aligned} \tag{7}$$

where functions $\mathcal{B}_2(\lambda,3;R)$ $(\lambda=1,3)$ are trivially identified from Eqs. (2) and (3), and that both scale like R^{-4}. Generally, for any spectroscopic process or property of rank r, functions $\mathcal{B}_r(\lambda,l;R)$ are computed as coefficients in the expansion of the $F \leftarrow I$ transition amplitude over convolution products $\{C_a^{(\lambda)} \otimes C^{(l)}\}^{(r)}$, with running indices λ and l.

1. The zeroth moment $M_0^{(2)}$

Accordingly, $M_0^{(2)}$ is expressed as the statistical average

$$\begin{aligned} M_0^{(2)} = \Bigg\langle & \sum_{\lambda_1\lambda_2 L} \mathcal{B}_2(\lambda_1,3;R)\mathcal{B}_2(\lambda_2,3;R) \\ & \times (\{C_a^{(\lambda_1)} \otimes C^{(3)}\}^{(2)}, \{C_a^{(\lambda_2)} \otimes C^{(3)}\}^{(2)}) \\ & \times (C_a^{(L)}, C^{(L)}) G_L(R) \Bigg\rangle, \end{aligned} \tag{8}$$

where $\lambda_1,\lambda_2 = 1,3$.

By using the recoupling technique of Ref. [21], we are now coupling $C_a^{(\lambda_1)}$ and $C_a^{(\lambda_2)}$ into $C_a^{(g)}$, and also, $C^{(3)}$ and $C^{(3)}$ into $C^{(g)}$, and we are then taking advantage of the remarkable property $(2L+1)\int\int (C^{(g)}, C_a^{(g)})(C^{(L)}, C_a^{(L)}) d\Omega d\Omega_a = 16\pi^2 \delta_{L,g}$. In so doing, $M_0^{(2)}$ is expressed as a linear combination

$$M_0^{(2)} = \sum_{\lambda_1\lambda_2 L} K_2(\lambda_1,3;\lambda_2,3;L) I_L(\lambda_1,3;\lambda_2,3) \tag{9}$$

of the radial integrals

$$I_L(\lambda_1,3;\lambda_2,3) = 4\pi \int G_L(R) \mathcal{B}_2(\lambda_1,3;R) \mathcal{B}_2(\lambda_2,3;R) R^2 dR \tag{10}$$

with weighting coefficients $K_2(\lambda_1,3;\lambda_2,3;L)$. The latter, in their most general form, read

$$\begin{aligned} & K_r(\lambda_1,l_1;\lambda_2,l_2;L) \\ & = (-1)^{\lambda_2+l_1} \Pi_{rr} \begin{Bmatrix} l_1 & l_2 & L \\ \lambda_2 & \lambda_1 & r \end{Bmatrix} \begin{pmatrix} \lambda_1 & L & \lambda_2 \\ 0 & 0 & 0 \end{pmatrix} \begin{pmatrix} l_1 & L & l_2 \\ 0 & 0 & 0 \end{pmatrix} \end{aligned} \tag{11}$$

with curly brackets and parentheses denoting $6j$ and $3j$ symbols, respectively.

For an isotropic potential, $L=0$. In that case only diagonal terms with $l_1=l_2\equiv l$; $\lambda_1=\lambda_2\equiv\lambda$ survive, and the $M_0^{(r)}$ moment of a r-rank property is reduced to a sum of positive integrals $I_0(\lambda,l;\lambda,l)$ with weighting coefficients $(2r+1)/(2l+1)(2\lambda+1)$. This result is in agreement with the formulas of the literature [7,22].

2. The second moment $M_2^{(2)}$

Here, $p=1$ and the moment is a velocity-dependent quantity. To derive $M_2^{(2)}$ the foregoing recoupling technique is used along with the useful expression

$$\frac{d}{dt} = (\mathbf{v},\boldsymbol{\nabla}) + (\mathbf{v}_a,\boldsymbol{\nabla}_a). \tag{12}$$

Quantities $\mathbf{v}$ and $\mathbf{v}_a$ denote velocities $\dot{\mathbf{R}}$ and $\dot{\mathbf{n}}_a$, respectively, whereas $\boldsymbol{\nabla}$ and $\boldsymbol{\nabla}_a$ stand for the gradient operators in the corresponding configuration subspaces. Note that $\mathbf{v}_a$ is purely rotational because CO_2 is bound. Unlike, translational velocity $\mathbf{v}$ has two components, a radial and an angular, to account for the relative motion of the two unbound colliders.

Let us now apply the time-derivative operator to $(\Delta\alpha^{(2)})_{FI}$, and then square and average the resulting expression. A Maxwell-Boltzmann velocity distribution is so introduced, as expected for properties that are velocity dependent. Obviously, any cross-term contributions due to the mixed terms so appearing (bilinear in $\mathbf{v}$ and $\mathbf{v}_a$) are washed out by the subsequent averaging operation, since classical distributions do not depend on the orientation of $\mathbf{v}$ or $\mathbf{v}_a$. The result reads as a simple sum $M_2^{(2)} = M_{2,T}^{(2)} + M_{2,R}^{(2)}$, where $M_{2,T}^{(2)}$ and $M_{2,R}^{(2)}$ are the translational and rotational contributions emerging from the first and second terms of Eq. (12), respectively.

Translational contribution $M_{2,T}^{(2)}$. Upon the decoupling of $\mathbf{v}$, quantity $(\mathbf{v},\boldsymbol{\nabla})(\Delta\alpha^{(2)})_{FI}$ becomes

$$(\mathbf{v},\boldsymbol{\nabla})(\Delta\alpha^{(2)})_{FI}=\sum_{hg\lambda}(-1)^{\lambda+g+h}\begin{Bmatrix}1 & 3 & g\\ \lambda & h & 2\end{Bmatrix}\times\{v^{(1)}\otimes\{C_a^{(\lambda)}\otimes\Phi_l^{(g)}\}^{(h)}\}^{(2)} \quad (13)$$

where

$$\Phi_l^{(g)}=\{\boldsymbol{\nabla}^{(1)}\otimes\mathcal{B}_2(\lambda,3;R)C^{(3)}\}^{(g)}, \quad (14)$$

$v^{(1)}=\mathbf{v}$, and $\boldsymbol{\nabla}^{(1)}=\boldsymbol{\nabla}$ $(\lambda=1,3)$.

As expected from the structure of $\dot{\mathbf{R}}$, the squaring of $(\mathbf{v},\boldsymbol{\nabla})(\Delta\alpha^{(2)})_{FI}$ results into a radial term, into an angular term, and into mixed terms. Use is made once again of the statistical independence of the translational variables $\mathbf{v}$ and $\mathbf{R}$, that cancels out the latter terms in the subsequent averaging. Final expressions for $M_{2,T}^{(2)}$ are obtained only after tedious algebra, that closely follows the calculus of Ref. [14], and use of the classical kinematic property $\mu_{a-b}\langle(\mathbf{v},\mathbf{v})\rangle=3k_BT$ (μ_{a-b} stands for the CO_2-Ar reduced mass) and the general coupling formula

$$\langle(\{A^{(a)}\otimes B^{(b)}\}^{(c)},\{A^{(a)}\otimes B^{(b)}\}^{(c)})\rangle=\frac{(2c+1)}{(2a+1)(2b+1)}\langle(A^{(a)},A^{(a)})\rangle\langle(B^{(b)},B^{(b)})\rangle, \quad (15)$$

the latter being applicable to any two statistically-independent irreducible spherical tensors $A^{(a)}$ and $B^{(b)}$.

In so doing, two separate contributions, referred to as the *translational-radial* $M_{2,T}^{(2)(\mathrm{rad})}$ and the *translational-angular* $M_{2,T}^{(2)(\mathrm{ang})}$, are clearly identified:

$$M_{2,T}^{(2)}=\frac{k_BT}{\mu_{a-b}}\sum_{\lambda_1\lambda_2L}K_2(\lambda_1,3;\lambda_2,3;L)[I_L^{(\mathrm{rad})}(\lambda_1,3;\lambda_2,3)+F(3,3,L)I_L^{(\mathrm{ang})}(\lambda_1,3;\lambda_2,3)] \quad (16)$$

where $\lambda_1,\lambda_2=1,3$; $F(x,y,z)=\frac{1}{2}[x(x+1)+y(y+1)-z(z+1)]$, and $I_L^{(\mathrm{rad})}$, $I_L^{(\mathrm{ang})}$ are "radial" and "angular" integrals defined by

$$I_L^{(\mathrm{rad})}(\lambda_1,3;\lambda_2,3)=4\pi\int_0^\infty G_L(R)\frac{\partial\mathcal{B}_2(\lambda_1,3;R)}{\partial R}\frac{\partial\mathcal{B}_2(\lambda_2,3;R)}{\partial R}R^2dR, \quad (17a)$$

$$I_L^{(\mathrm{ang})}(\lambda_1,3;\lambda_2,3)=4\pi\int_0^\infty G_L(R)\mathcal{B}_2(\lambda_1,3;R)\mathcal{B}_2(\lambda_2,3;R)dR. \quad (17b)$$

It is particularly interesting that this separability remains valid whatever the degree of anisotropy of the potential, since no assumption was made as to the form of $V(\mathbf{R},\Omega_a)$. For isotropic potentials, $L=0$. In that case, again, diagonal terms with $l_1=l_2\equiv l$; $\lambda_1=\lambda_2\equiv\lambda$ are the only to survive, and $M_{2,T}^{(r)}$, in its most general form for any l and r values, reads

$$M_{2,T}^{(r)}=\frac{k_BT}{\mu_{a-b}}\sum_{l\lambda}\frac{2r+1}{(2l+1)(2\lambda+1)}\times[l(l+1)I_0^{(\mathrm{ang})}(\lambda,l;\lambda,l)+I_0^{(\mathrm{rad})}(\lambda,l;\lambda,l)] \quad (18)$$

It is gratifying that Eq. (18) matches exactly the result obtained by Poll and Hunt [23] for the particular case of translational collision-induced absorption spectra by atomic mixtures ($r=1$, $\lambda=0$).

Rotational contribution $M_{2,R}^{(2)}$. Same as before decoupling procedure is followed, which, for a typical $\{C_a^{(\lambda)}\otimes C^{(3)}\}^{(2)}$ $(\lambda=1,3)$ term of the CO_2-Ar polarizability, gives

$$(\mathbf{v}_a,\boldsymbol{\nabla}_a)\{C_a^{(\lambda)}\otimes C^{(3)}\}^{(2)}=-\Pi_\lambda^{-1}(-1)^\lambda\sum_{hg}\Pi_{hg}\begin{Bmatrix}1 & \lambda & g\\ 3 & h & 2\end{Bmatrix}\times[\lambda\sqrt{\lambda+1}\,\delta_{g,\lambda+1}+(\lambda+1)\sqrt{\lambda}\,\delta_{g,\lambda-1}]\times\{v_a^{(1)}\otimes\{C_a^{(g)}\otimes C^{(3)}\}^{(h)}\}^{(2)} \quad (19)$$

with $v_a^{(1)}=\mathbf{v}_a$.

We are now applying the recoupling technique [21], as we did it before. However, we keep in mind that, by contrast with the translational case in which $\mathbf{v}$ and $\mathbf{R}$ were uncorrelated, the relative orientation of $\mathbf{v}_a$ and $\mathbf{n}_a$ is fixed. Thus rotational-velocity and orientational averages no longer are independent quantities.

Going further, the square of $(\mathbf{v}_a,\boldsymbol{\nabla}_a)(\Delta\alpha^{(2)})_{FI}$ is reduced to a sum of terms that are proportional to $\{v^{(1)}\otimes v^{(1)}\}^{(g)}$ $(g=0,2)$, the value $g=1$ being forbidden. The treatment of the $g=0$ term can be made in the same way as the one used to derive the translational term, whereas a more complicated treatment shows that the $g=2$ term contributes half the one with $g=0$ (for details, see [14]). The resulting total rotational contribution becomes

$$M_{2,R}^{(2)}=\frac{k_BT}{\mathcal{I}}\sum_{\lambda_1\lambda_2L}K_2(\lambda_1,3;\lambda_2,3;L)F(\lambda_1,\lambda_2,L)I_L(\lambda_1,3;\lambda_2,3), \quad (20)$$

where $\mathcal{I}$ denotes the CO_2 moment of inertia and $I_L(\lambda_1,3;\lambda_2,3)$ is given by Eq. (10).

As before, for isotropic potentials ($L=0$) diagonal terms with $l_1=l_2\equiv l$; $\lambda_1=\lambda_2\equiv\lambda$ are the only to survive, and the corresponding contribution (in the most general case of arbitrary l and r) reads:

$$M_{2,R}^{(r)}=\frac{k_BT}{\mathcal{I}}\sum_{l\lambda}\frac{2r+1}{(2l+1)(2\lambda+1)}\lambda(\lambda+1)I_0(\lambda,l;\lambda,l). \quad (21)$$

It is worthwhile pointing out that at no step has the above analysis assumed some particular form of V. Thus, the moment expressions so obtained have now allowed the long overdue generalization of the properties to anisotropic potentials. Since the anisotropy of the CO_2-Ar potential, in particular, is known to give rise to new channels that have no analog in the one dimension, reducing V to a spherically

symmetric function would be ill-advised [24]. Proper account of the potential anisotropy is simply indispensable.

IV. EXPERIMENTAL

The scattering intensities were measured with a conventional Raman setup. For more details, see Ref. [13]. The $\lambda_L = 514.5$ nm Ar^+ laser green line was used along with a power of 2 *W* to excite the gaseous sample. Given that the laser beam polarization was by default perpendicular to the plane defined by the incident and the scattered beam wave vectors, a half-wave plate associated with a glan polarizer were put to make it possible to record depolarized spectra, $I_{\parallel}(\nu)$. A fused silica four-window high-pressure cell was used for the room temperature gaseous sample. The scattered radiation (at a right angle relative to the incident beam) was analyzed with a double monochromator with holographic gratings. The resolution was fixed at 1.2 cm^{-1}. For signal detection, a nitrogen-cooled multichannel charged coupled device (CCD) associated with a holographic super notch filter was employed. To extract binary cross sections, the dependence of the total signal was studied as a function of both the CO_2 and Ar sample working densities ρ_a and ρ_b, for every value of the probed Raman frequency ν, along with the constraint of a constant CO_2:Ar concentration ratio $\frac{\rho_a}{\rho_b} = \gamma$. Specifically, the scattering signal $I(\nu, \rho_a, \rho_b)$ was viewed as a double power series expansion in ρ_a and ρ_b,

$$I(\nu,\rho_a,\rho_b) = I_0(\nu) + I_1^a(\nu)\rho_a + I_1^b(\nu)\rho_b + I_2^{aa}(\nu)\frac{\rho_a^2}{2!} + I_2^{ab}(\nu)\rho_a\rho_b + I_2^{bb}(\nu)\frac{\rho_b^2}{2!} + I_3^{aaa}(\nu)\frac{\rho_a^3}{3!} + \cdots \quad (22)$$

with ν-dependent coefficients of particular physical meaning. The first term $I_0(\nu)$ was related to the dark noise of the CCD. The coefficient $I_1^a(\nu)$, identified as the signal owing to CO_2 monomers, was found to be negligible. This was an expectable result, the primary cause of which is due to the Raman inactivity of the antistretching CO_2 mode that prevents the observability of any electric dipole-electric dipole spectrum. Note, however, that when accounting for virtual electric dipole-electric quadrupole transitions or/and for electric dipole-magnetic dipole transitions, allowed CO_2 Raman spectra are expected to occur. Although the latter exhibit a linear dependence on ρ_a and they must formally contribute to $I_1^a(\nu)$, this contribution was found to be small because it originates from high-order multipolar processes. These spectra are not collision-induced ones and, whatever their magnitude, are irrelevant to our study. A vanishingly weak signal $I_1^b(\nu)$, owing to scattering by single atomic argon, was detected in the frequency range of interest, and the same was true for $I_2^{bb}(\nu)$. The fourth and fifth terms of Eq. (22), scaling quadratically with density, were interpreted as being due to pairwise interactions in the frequency range of interest, and the corresponding cross section yielded the binary spectrum of the gas. Higher-order terms involving $I_3^{aaa}(\nu)$, $I_3^{aab}(\nu)$, $I_4^{aaaa}(\nu)$, … represent ternary (or higher-order) spectra that are generated by many-body collisions.

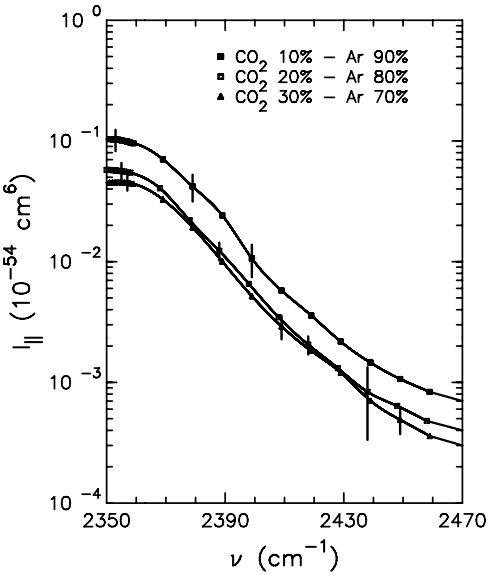

FIG. 3. Experimental absolute-unit binary depolarized CIRS spectra $I_{\parallel}$ (cm^6) of a CO_2 mixture with Ar, as a function of ν (in cm^{-1}), in the interval $2350 \leqslant \nu \leqslant 2470$ cm^{-1}, and for CO_2:Ar concentrations amounting to 10:90 (■); 20:80 (□); 30:70 (▲). Curves correspond to a spline smoothing of the experimental data.

Having identified the physically relevant binary component I_2, we cast it into the form $I_2(\nu,\rho_a) = \left[I_2^{aa}(\nu) + I_2^{ab}(\nu)\frac{2}{\gamma}\right]\frac{\rho_a^2}{2}$. In so doing, we were able to isolate the density-independent quantity inside the brackets and to calibrate it properly. The resulting calibrated binary depolarized signal is formally expressed as $I_{\parallel}^{\text{mix}} = I_{\parallel}^{aa}(\nu) + I_{\parallel}^{ab}(\nu)\frac{2}{\gamma}$, allowing the determination of the desired CO_2-Ar spectrum

$$I_{\parallel}^{ab}(\nu) = (I_{\parallel}^{\text{mix}} - I_{\parallel}^{aa})\frac{\rho_a}{2\rho_b}. \quad (23)$$

Here, pure, gaseous, room-temperature carbon dioxide was used at first, and the ν_3 band of CO_2 (centered at $\nu_0 = 2350$ cm^{-1}) was recorded. Then, the same spectral domain was probed for three gaseous mixtures with argon, for CO_2 concentrations $\gamma/1+\gamma$ amounting to 10%, 20%, and 30%. The detection was made within the spectral side $\nu \geqslant \nu_0$, that is, for $\nu_2 \leqslant \nu_1 - \nu_0$, so that the signal benefits from a natural enhancement due to the asymmetry of the band. However, given the almost exponential decrease of the intensity with increasing detuning, the asymmetry of the profile was found to affect the low-order moments only slightly. Densities were deduced from $\mathcal{P}V$ measurements against pressure $\mathcal{P}$, with temperature T treated as a parameter (for pure CO_2, see Refs. [25–27]; for pure argon, see Refs. [28,29]; for the mixture, see Ref. [28]). According to a procedure described elsewhere [13], scattering cross sections were calibrated on an absolute scale. To this purpose, the well known integrated cross section of the S_0 (1) rotational line of hydrogen was used as an external reference.

V. RESULTS

A. Experimental

The lower bound of the explored spectral domain was fixed at the top of the ν_3 band. Scattering intensities were

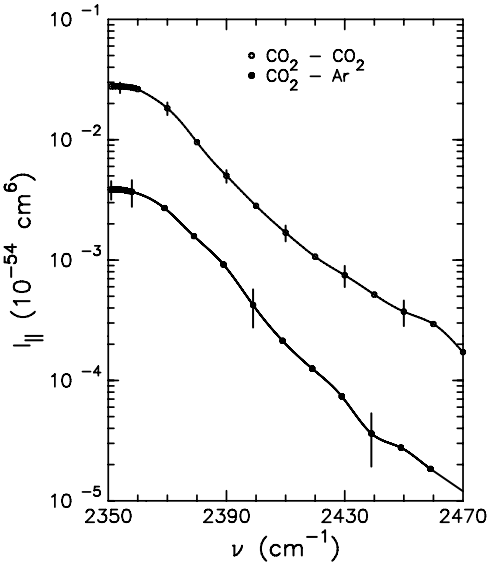

FIG. 4. Experimental absolute-unit depolarized CO_2-CO_2 (○) and CO_2-Ar (●) CIRS spectra of the ν_3 CO_2 band, as a function of ν (in cm^{-1}). Curves correspond to a spline smoothing of the experimental data.

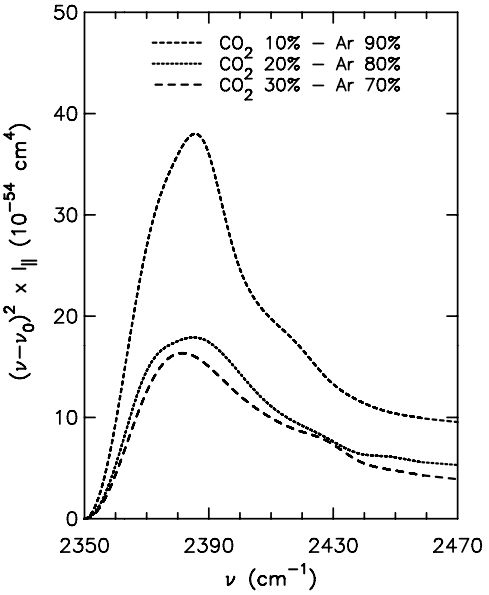

FIG. 5. Same as in Fig. 3 but for the quantity $(\nu-\nu_0)^2\times I_\parallel$, as a function of ν.

recorded for the three gaseous mixtures with argon and for pure CO_2, up to $\nu=2460\ cm^{-1}$, that is, over detunings of $110\ cm^{-1}$. We were unable to go farther into the wing because of the presence of a multitude of spectral lines. The three recorded spectra are shown in Fig. 3, allowing for a meaningful critical comparison. A symmetrization procedure was applied to the recorded spectrum in order to mimic the truly classical profile, and then low-order spectral moments M_{2p}^s $(p=0,1)$,

$$M_{2p}^s = \frac{15}{2}\left(\frac{\lambda_{L0}}{2\pi}\right)^4 (2\pi c)^{2p}\int_{-\infty}^{\infty} I_\parallel^s(\nu)(\nu-\nu_0)^{2p}d\nu \qquad (24)$$

with $\lambda_{L0}^{-1}=\lambda_L^{-1}-\lambda_0^{-1}$, were extracted from the recorded spectra, for pure CO_2 ($s=CO_2$-CO_2) and for its mixtures with argon ($s=$mix). Zeroth and second moments for CO_2-Ar were then deduced according to the relationship

$$M_{2p}^{CO_2\text{-Ar}} = (M_{2p}^{\text{mix}} - M_{2p}^{CO_2\text{-}CO_2})\frac{\rho_a}{2\rho_b}, \qquad (25)$$

where $\frac{\rho_a}{\rho_b}=\frac{10}{90}, \frac{20}{80}, \frac{30}{70}$ designates the CO_2:Ar working concentration ratios. In order to provide converged integrals of Eq. (24), a pure exponential function fitting the monotonous profile was used to extrapolate $I_\parallel^s(\nu)\times(\nu-\nu_0)^{2p}$ above $2460\ cm^{-1}$. The relative contribution to M_0^s and M_2^s due to the extrapolation amounted to 0.5 and 9%, respectively, whereas the impact of the natural asymmetry of the profile to M_0^s and M_2^s was found to be much smaller than the experimental uncertainty.

Figure 4 shows the extracted CO_2-Ar spectrum as a function of ν, along with the CO_2-CO_2 spectrum for comparison. For the extraction of $I_\parallel^{CO_2\text{-Ar}}$, the expression of Eq. (23) containing $I_\parallel^{\text{mix}}$ and $I_\parallel^{CO_2\text{-}CO_2}$, in a way analogous to the one Eq. (25) does it for moments, was used. Binary collisions between CO_2 and Ar turned out to be less effective, by a factor of six, than collisions between like CO_2 molecules. As is seen from Fig. 4, above $\nu\approx 2380 cm^{-1}$, the spectrum of CO_2-Ar exhibits an almost pure exponential dependence, whereas for pure CO_2, the relative decrease of the intensity is slower asymptotically. Clearly, this property once more demonstrates that CIRS spectra at large detunings deviate from ordinary Gaussian profiles and may significantly affect any spectral structure that is located at much farther frequencies.

Figures 5 and 6 show how the function $(\nu-\nu_0)^2\times I_\parallel^s(\nu)$ behaves with ν, both for the gaseous mixtures ($s=$mix) and for the binary encounters ($s=CO_2$-CO_2 and $s=CO_2$-Ar),

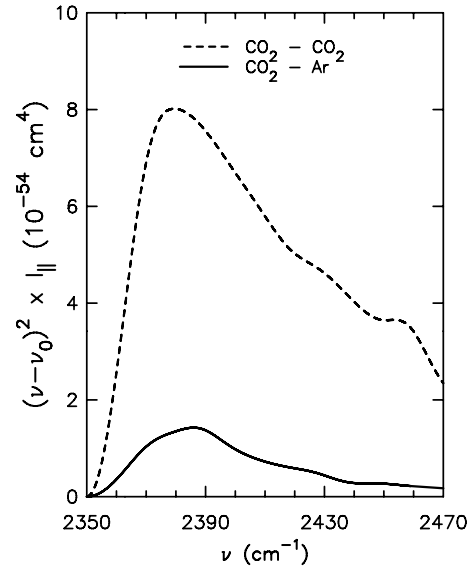

FIG. 6. Same as in Fig. 4 but for the quantity $(\nu-\nu_0)^2\times I_\parallel$, as a function of ν.

TABLE II. The CO_2-Ar zeroth anisotropic moment, $M_0^{(2)}$ (in a_0^9), second anisotropic moment, $M_2^{(2)}$ (in $10^{24}a_0^9\,\mathrm{sec}^{-2}$), and square-rooted reduced second anisotropic moment, $(\bar{M}_2^{(2)})^{1/2}$ (in cm^{-1}). The contributions (in %) of the various degrees of freedom that are relative to $M_2^{(2)}$ are also shown in the specific case where the SCF data from [16] were used (middle column). For MP2 the % contributions were found to be identical (not shown).

	Theory (this work)		
	Amos *et al.*[a] SCF	Haskopoulos-Maroulis[b] SCF	Haskopoulos-Maroulis[b] MP2
	DIQ	DIQ	DIQ
$M_0^{(2)}$	2.17	6.02	8.18
$M_2^{(2)}$	57.6	159.9	216.0
		$M_{2,R}^{(2)}$ $M_{2,T}^{(2)(\mathrm{rad})}$ $M_{2,T}^{(2)(\mathrm{ang})}$	
		58% 23% 19%	
$(\bar{M}_2^{(2)})^{1/2}$	27.3	27.3	27.3
	DIQ+NLD	DIQ+NLD	DIQ+NLD
$M_0^{(2)}$	0.27	2.11	3.45
$M_2^{(2)}$	10.2	56.2	91.0
$(\bar{M}_2^{(2)})^{1/2}$	32.6	27.4	27.2
	Experiment (this work)		
	$M_0^{(2)}=3.75\pm0.6$		
	$M_2^{(2)}=90.6\pm19.8$		
	$(\bar{M}_2^{(2)})^{1/2}=27.9\pm3.8$		

[a]With input data from [5].
[b]With input data from [16].

respectively. The moment values so obtained are shown in Table II along with the results from theoretical calculations (see below). Uncertainties in the reported values took into account experimental error bars and estimated extrapolation errors.

B. Theoretical

Based on the developed theory, the zeroth moment values were obtained both by using the irreducible spherical tensor (IST) formalism [Eq. (9)] and with straightforward numerical integration in the collision frame. Practically identical results were obtained. For the second moment, the IST expressions of Eqs. (16) and (20) were applied. A FORTRAN code was developed for the purpose. The best to date CO_2-Ar PES, notoriously known for being optimized against a multitude of physical properties and for exhaustively accounting for the pronounced anisotropy of the system, was employed [12]. Both versions of the potential (single-site and two-site repulsion models) were checked and negligible discrepancies were found ($<1\%$). The presence of the anisotropic terms ($L\neq0$) in the binary correlation function turned out to be responsible for a decrease by 20–25% of the zeroth and second moments, clearly showing that the anisotropy of the potential must be crucial for a realistic spectrum modeling. However, this anisotropy did not manifest itself as strikingly as did it in the torque moment case [14], where a dramatic contribution, almost canceling that of the isotropic $L=0$ term, had been found.

Values of input parameters α_b and $(\mu_a)_{f_a i_a}$, deduced from the experiment [18], were reliable to within 1%. For B_b, fully correlated *ab initio* computations provided an accuracy to within 5% [17]. In contrast, early SCF data on both the vibrational dipole moment and the dipole-quadrupole polarizabilities $\hat{A}$ turned out to be much less reliable. Specifically, according to Ref. [5], the accuracy of the SCF CO_2 dipole moment derivative with respect to the antisymmetric stretching coordinate was estimated to within 20%. This significant lack of accuracy (as compared to other quantities which are better known) can be explained by the generally strong dependence that linear and nonlinear polarizabilities are known to exhibit on multielectron densities; as refined calculations have demonstrated, polarizabilities are less reliable than dipole moments for a given optimization level [30], and any possible success of the early SCF data along with the physically insufficient DIQ model would not be but accidental (see below).

Upon comparison of the two sets of SCF data of Table I for the CO_2 vibrational dipole-quadrupole polarizabilities [5,16], the conclusion is drawn that increase of the basis drastically improves accuracy. For MP2, however, despite its high degree of sophistication as compared to SCF, certain data by Haskopoulos and Maroulis show quite a large deviation from coupled-cluster single, double, and connected triple excitation response approach [CCSD(T)] results (the case of the vibrational dipole-dipole-dipole polarizability). Besides, MP2 predicts a vanishing vibrational matrix ele-

ment $(a_{3a})_{f_a i_a}$, a result that is hard to justify on physical grounds. The need for more accurate MP2 $(A_{Z,ZZ})_{f_a i_a}$ and $(A_{X,ZX})_{f_a i_a}$ parameters is also corroborated by preliminary experimental results on the isotropic CO_2-Ar spectrum that prompt the polarized component $(a_{3a})_{f_a i_a}$ to take a small yet definitely nonzero value.

Optimization level and sophistication of the basis employed were found to dramatically affect the response of the scattering amplitude. Thus, according to the $M_0^{(2)}$ entries of Table II, the earlier SCF data [5] predict that DIQ would be insufficient by 70% to explain the integrated intensity of the band. This great mismatch is getting huge upon inclusion of the new NLD polarization of Eq. (3) (see also paper I), found to strongly and destructively interfere with DIQ. The reduced accuracy of the earlier SCF data on $(a_{1a})_{f_a i_a}$ and $(a_{3a})_{f_a i_a}$, along with a lack of CIRS measurements, may explain why the NLD mechanism had thus far escaped attention. Remarkably, once state-of-the-art MP2 data [16] are used along with an exhaustive calculation for both DIQ and NLD mechanisms, agreement between theoretical and experimental zeroth moments is obtained. We point out that the result is particularly sensitive to the accuracy of the entry data because of the strong interplay between antagonistic contributions owing essentially to the two $\{C_a^{(1)} \otimes C^{(3)}\}^{(2)}$ terms of Eqs. (2) and (3), as seen from the relative signs of the entry quantities. Again, the disappointing prediction of the SCF integrated intensity, which is far off the experimental tolerance, lies with the (probably too large) value for $(a_{1a})_{f_a i_a}$. Interestingly, although MP2 and SCF $(a_{1a})_{f_a i_a}$ values by Haskopoulos and Maroulis differ from each other by less than 15% (which is a rather common discrepancy in *ab initio* computations of properties involving derivatives with respect to vibrational coordinates), its impact on $M_0^{(2)}$ was found to exceed 50%, that is a huge, well measurable deviation.

Table II also gathers values of the second moment, $M_2^{(2)}$, for the earlier and recent *ab initio* data of Table I and with inclusion or not of the NLD effect. Once again, a spectacular agreement between theory and experiment is observed, provided that all predicted mechanisms were included and state-of-the-art MP2 data were input. Similar conclusions to those for $M_0^{(2)}$ are drawn as to the inadequacy of the earlier results by Amos *et al.* and the underestimating response of the SCF recent computations.

In order to quantify the degree of adequacy of the early SCF calculation for $(a_{3a})_{f_a i_a}$ [5] (see Table I), the square-rooted reduced second moment $(\bar{M}_2^{(2)})^{1/2}$ was found to be a good probe, as it is known to correlate with the half-width of the spectrum [31]. In this respect, the presence of the second term of Eq. (2), that scales like the third-rank harmonics of the molecular axis orientation, substantially increases the rotational contribution to the reduced second moment. Table II shows $(\bar{M}_2^{(2)})^{1/2}$ for the various *ab initio* data, with and without account of the NLD mechanism. Clearly, for the complete DIQ+NLD polarization, the early SCF data predict a quantity that is inconsistent with the observation. This discrepancy indicates that these data are insufficient, not only for static properties (absolute moments) but also for (dynamical) shape characteristics. It is worthwhile noting that the experimental $(\bar{M}_2^{(2)})^{1/2}$ value of Table II is compatible with the truly measured half-width of the experimental spectrum, $\approx 27\ \mathrm{cm}^{-1}$ (Fig. 4), even though the latter is by no means a Gauss function in the tail.

The second moment consists of terms accounting for both angular and radial translational motions, and for molecular rotation. In the middle-column of Table II are shown the contributions of the various degrees of freedom to the second moment, obtained with the most recent SCF data [16]. For MP2, the % contributions were found to be identical to those for SCF and are not shown. The rotation of the CO_2 molecule was found to be responsible for the largest part (58%) of the second moment. The rest, distributed as a translational degree of freedom to the unbound CO_2-Ar colliders, was found to be almost equally shared by the intrinsic radial (23%) and angular (19%) degrees of freedom.

In view of the feasibility of highly accurate CIRS experiments on complex systems (such as the done here on CO_2 embedded in a rare-gas environment) and of the possibility to calculate rigorous spectral moments (by means of the mathematical expressions of Sec. III), our methodology appears as an original, sensitive device for predicting the values of a small number of polarizability parameters.

VI. SYNOPSIS AND OUTLOOK

The CO_2-Ar collision-induced Raman scattering process was both theoretically and experimentally studied in the spectral domain of the strong IR-active CO_2 ν_3 transition. Zeroth and second anisotropic moment expressions were obtained by using the IST formalism and an exhaustive mathematical input for the incremental polarizability matrix-elements $(\Delta\alpha^{(2)})_{FI}$. The latter, obtained by means of a recently reported diagrammatic method, turns out to include a nonlinear effect (NLD) owing to the vibrating dipole of CO_2 that (nonlinearly) polarizes the atomic perturber. Through an exhaustive comparison with depolarized CO_2-Ar spectra, extracted from careful measurements on pure CO_2 gas and its mixture with Ar, we provided evidence of a substantial contribution of the latter term to the scattering cross-sections. For this purpose, the full anisotropy of the CO_2-Ar potential had to be considered, and an exhaustive account of accurate dipole moment, polarizability and hyperpolarizability values for the interacting species be taken. A spectacular agreement between theory and experiment is obtained, provided that state-of-the-art MP2 values of dipole-quadrupole polarizability matrix-elements $(A_{Z,ZZ})_{f_a i_a}$ and $(A_{X,ZX})_{f_a i_a}$ were input. Our findings clearly show that the CO_2-Ar collision-induced ν_3 band of CO_2 is the result of a delicate interplay between the NLD mechanism and the well-known DIQ polarization. Besides, as regards the dynamics of the process, it was shown that most of the integrated cross section comes from the rotation of the CO_2 molecule, whereas the rest of the intensity is equally shared by the radial and angular motions of the translating unbound colliders. The sensitivity of the zeroth and second moments, which

is due to the unprecedented heaviness of the mixing between DIQ and NLD interactions, suggests that our theoretical treatment, along with careful collision-induced measurements over extended spectral domains, can be a useful, general methodology and a sensitive tool for predicting insufficiently known vibrational terms of mixed polarizabilities.

ACKNOWLEDGMENTS

This work was done as a collaborative project between the University of Angers and the Saint Petersburg State University. The authors acknowledge support from the Laboratoire POMA, UMR CNRS 6136.

[1] L. Frommhold, Adv. Chem. Phys. **46**, 1 (1981).
[2] A. Borysow and L. Frommhold, Adv. Chem. Phys. **75**, 439 (1989).
[3] *Collision- and Interaction-Induced Spectroscopy*, Vol. 452, NATO ASI Series C: Mathematical and Physical Sciences, edited by G. C. Tabisz and M. N. Neuman (Kluwer Academic, Dordrecht, 1995).
[4] P. Kaatz and D. P. Shelton, Mol. Phys. **88**, 683 (1996).
[5] R. D. Amos, A. D. Buckingham, and J. H. Williams, Mol. Phys. **39**, 1519 (1980).
[6] V. Teboul, Y. Le Duff, and T. Bancewicz, J. Chem. Phys. **103**, 1384 (1995).
[7] T. I. Cox and P. A. Madden, Mol. Phys. **39**, 1487 (1980).
[8] A. P. Kouzov, M. Chrysos, F. Rachet, and N. I. Egorova, Phys. Rev. A **74**, 012723 (2006).
[9] J. F. Ward, Rev. Mod. Phys. **37**, 1 (1965).
[10] P. W. Langhoff, S. T. Epstein, and M. Karplus, Rev. Mod. Phys. **44**, 602 (1972).
[11] As optical transitions in CIRS are mainly due to continuum-continuum interactions, the resulting spectra are broad bands whose widths far exceed the typical magnitudes of the neglected effects. In the case of nonpolar particles, in particular, such as the CO_2 molecule or the Ar atom treated here, some of the formally missing effects are strictly zero as a consequence of the vanishing expectation values of the dipole moments for both colliders.
[12] J. M. Hutson, A. Ernrsti, M. M. Law, C. F. Roche, and R. J. Wheatley, J. Chem. Phys. **111**, 9130 (1996).
[13] F. Rachet, Y. Le Duff, C. Guillot-Noël, and M. Chrysos, Phys. Rev. A **61**, 062501 (2000).
[14] A. P. Kouzov, Mol. Phys. **94**, 627 (1998).
[15] Notation ν_1 and ν_2 for photon frequencies should not be confused with the denomination for the CO_2 symmetric-stretching or bending transitions, bands, or modes.
[16] A. Haskopoulos and G. Maroulis, Chem. Phys. Lett. **417**, 235 (2006).
[17] S. Coriani, C. Hättig, and A. Rizzo, J. Chem. Phys. **111**, 7828 (1999).
[18] T. D. Kolomiitzova, A. V. Liaptzev, and D. N. Schepkin, Opt. Spectrosc. **88**, 719 (2000).
[19] Note that even if the all-orders intermolecular interaction $W=\Sigma_{l_a l_b} W_{l_a l_b}$, were included in the analysis, V would still be different from W, because of short-range exchange contributions and asymptotic retardation effects, unaccounted for in the diagrammatic formalism of Ref. [8].
[20] To the best of our knowledge, the anisotropy of the interaction potential has been analytically accounted for only by Cox and Madden [7], who derived $M_0^{(2)}$ for a particular (DID) case. How the anisotropy of the potential affects $M_2^{(2)}$ had thus far been an open question.
[21] D. A. Varshalovich, A. N. Moskalev, and V. K. Khersonskii, *Quantum Theory of Angular Momentum* (World Scientific, Singapore, 1988).
[22] T. Bancewicz, V. Teboul, and Y. Le Duff, Mol. Phys. **81**, 1353 (1994).
[23] J. D. Poll and J. L. Hunt, Can. J. Phys. **54**, 461 (1976).
[24] S. E. Lokshtanov, S. V. Ivanov, and A. A. Vigasin, J. Mol. Struct. **742**, 31 (2005).
[25] A. Michels and C. Michels, Proc. R. Soc. London, Ser. A **153**, 201 (1935).
[26] E. G. Butcher and R. S. Dadson, Proc. R. Soc. London, Ser. A **277**, 448 (1964).
[27] R. S. Dadson, E. J. Evans, and J. H. King, Proc. Phys. Soc. London **92**, 1115 (1967).
[28] R. N. Lichtenthaler and K. Schäfer, Ber. Bunsenges. Phys. Chem. **73**, 42 (1969).
[29] A. L. Blancett, K. R. Halland, and F. B. Canfield, Physica (Utrecht) **47**, 75 (1970).
[30] G. Maroulis and A. J. Thakkar, J. Chem. Phys. **93**, 4164 (1990).
[31] The reduced second moment (in cm^{-2}) is defined by $\bar{M}_2^{(2)} = (2\pi c)^{-2} M_2^{(2)} / M_0^{(2)}$. For Gaussian band shapes, its square root provides the half-width (in cm^{-1}) at near half maximum.